Journal of Innovative Optical Health Sciences
Vol. 9, No. 4 (2016) 1630006 (20 pages)

DOI: 10.1142/S1793545816300068

World Scientific
www.worldscientific.com

Upconversion nanoparticle as a theranostic agent for tumor imaging and therapy

Wenkai Fang* and Yanchun Wei†
Ministry of Education Key Laboratory of Laser Life Science & Institute of Laser Life Science College of Biophotonics South China Normal University Guangzhou 510631, P. R. China
**fwkoneway@163.com*
†*weiyanchun@scnu.edu.cn*

Received 14 November 2015
Accepted 2 March 2016
Published 16 May 2016

Upconversion nanoparticles (UCNPs) as a promising material are widely studied due to their unique optical properties. The material can be excited by long wavelength light and emit visible wavelength light through multiphoton absorption. This property makes the particles highly attractive candidates for bioimaging and therapy application. This review aims at summarizing the synthesis and modification of UCNPs, especially the applications of UCNPs as a theranostic agent for tumor imaging and therapy. The biocompatibility and toxicity of UCNPs are also further discussed. Finally, we discuss the challenges and opportunities in the development of UCNP-based nanoplatforms for tumor imaging and therapy.

Keywords: Laser; upconversion material; bioimaging; toxicity.

1. Introduction

Optical imaging is an important technique used in the field of biomedical research because of its non-invasive, real-time and high magnification characteristics. Researchers have demonstrated various luminescence materials for optical bioimaging such as fluorescent proteins,[1] organic dyes,[2,3] metal complexes,[4] gold nanorods[5] and semiconductor quantum dots (QDs).[6,7] Most of these fluorescence probes are based on single-photon excitation mechanism. In the bioimaging application of them, there are some limitations existing, including the low optical penetration depth in tissues, low signal-to-noise ratio (SNR) caused by auto-fluorescence from the biological tissue, and the cell damage caused by the high-energy photons.

Comparing conventional fluorescence materials, an excellent imaging probe which is based on

†Corresponding author.

upconversion luminescence (UCL) mechanism, is developed. UCL is an anti-Stokes' emission process by converting long wavelength irradiation into shorter wavelength light emission, such as near infrared light (NIR) to shorter NIR, visible (blue, green, red), or UV. Up to now, the efficient upconversion luminescence only occurred in the compounds doped with rare earth ions. In particular, under continuous wave (CW) excitation at NIR, lanthanide(Ln)-doping upconversion nanoparticles (UCNPs) exhibit unique UCL properties, such as sharp emission line, long lifetime, a large anti-Stokes shift of several hundred nanometers, superior photostability and nonblinking.[8] The UCL has several attractive pionts for bioimaging: one is that the NIR light excitation does less harm to the living cells; the second, high SNR due to the very low auto-fluorescence with the NIR excitation; third, the deep tissue penetration owing to the excitation and emission wavelengths both in the range of the biological optical window. Based on the advantages, UCNPs have been successfully studied applying in a wide biomedical fields, including cell tracking, lymphatic imaging, vascular imaging, tumor targeted imaging and therapy.

Theranostics is defined as the increasingly close link between diagnostics and therapy. The objective of theranostics is to enable the proper therapy via a right diagnostics to patients.[9] Therefore, theranostics for tumor treatment is proposed to realize effective treatment.[10,11] Owing to the unique optical character, UCNPs represent an excellent biological platform for diagnostics and tumor targeted therapy, and is a hopeful candidate for theronostic agent. In this review, we summarize the recent progress as regards the using of UCNPs for tumor imaging and therapy and give a prospect on bio-application of this promising material.

2. UCL Mechanism of the Lanthanide-Doped Nanophosphors

UCL has a very different luminescence mechanism comparing to conventional fluorophore. The excited state absorption (ESA) of UCNPs had already been demonstrated in papers.[12] ESA takes the form of successive absorption of pump photons by a single ion and achieves high state due to the ladder-like structure of a simple multilevel system. Then, the ion releases its energy by emitting a photon and returns to the ground state (Fig. 1(a)). With a rapid development of spectroscopy, more upconversion mechanisms were discovered. Energy transfer upconversion (ETU) was first observed in Yb^{3+}–Tm^{3+} co-doped glass.[13] In ETU, a sensitized ion 1 sequentially provides energy for ion 2 as activator by the energy transfer process.[14,15] The activator is excited to a higher state from which anti-Stokes emission originates (Fig. 1(b)).[16] Around the same time, the cooperative sensitization[17] (CSU) and cooperative luminescence[18] upconversion mechanisms were also discovered. In cooperative sensitization, two ions as sensitizers simultaneously transfer energy to an activator. The activated ion achieves a real excited state where upconverted luminescence occurs (Fig. 1(c)). Cooperative luminescence is the same as the cooperative sensitization except that the emitting state replaces the intermediate state. Besides the above, further possible upconversion mechanisms still is being proposed and studied.[19]

To implement the upconversion energy transfer as the above, the constructed UCNPs generally contain three parts: host, sensitizer and activator. The selection of host could influence the intensity of luminescence. An ideal host material should have low nonradiative losses and high radiative emission. Many compounds, such as oxides (Y_2O_3, ZrO_2, Gd_2O_3, La_2O_3, Lu_2O_3), fluorides ($NaYF_4$, $NaYbF_4$, $NaLaF_4$, LaF_3, GdF_3), phosphates, heavy halides (GdOCl), oxysulfide (Y_2O_2S), vanadates (YVO_4, $GdVO_4$), have been studied as the host lattice for UCL.[20–28] Following the researches, the fluorides have become the most famous host materials due to their low photon energies and high chemical stability. By selection of activators with different energy level distribution, various wavelength emission can be obtained. Hexagonal $NaYF_4$:Yb^{3+}/Er^{3+} usually exhibits green emission located at 510–570 nm ($^2H_{11/2}$+$^4S_{3/2}$ → $^4I_{15/2}$) and red emission located at 630 and 660 nm ($^2F_{9/2}$ → $^4I_{15/2}$). For Yb^{3+}, Tm^{3+} co-doped UCNPs, its emissions center at 451 ($^1D_2$ → $^3F_4$), 481 ($^1G_4$ → $^3H_6$), 646 ($^1G_4$ → $^3F_4$) and 800 nm ($^3H_4$ → $^3H_6$). $NaYF_4$:Yb^{3+}/Er^{3+} and $NaYF_4$:Yb^{3+}/Tm^{3+} have been widely studied for tumor imaging and therapy *in vivo*.

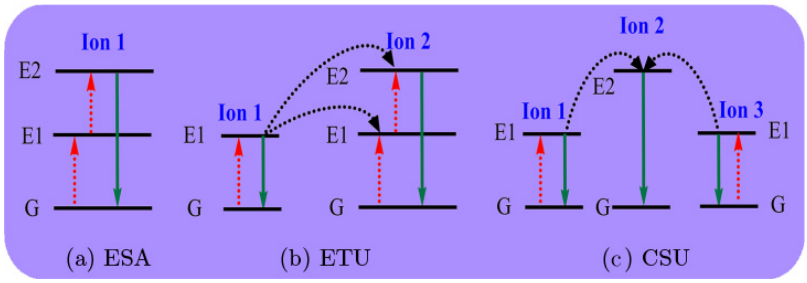

Fig. 1. Principles of UCL process for lanthanide-doped UCNPs. (a) ESA, (b) ETU and (c) CSU.

3. Synthesis of UCNPs

3.1. *Synthetic methods of UCNPs*

Development of facile synthesis methods for high-quality UCNPs with suitable size, uniform shape, controlled composition and crystalline phase are important to tune their chemical and optical properties for imaging and therapy. To date, a range of synthetic approaches, such as hydro(solvo)thermal process, thermal decomposition, *one-pot template-free synthesis*, sol–gel process, Ostwald-ripening method, and coprecipitation method, have been devoted to synthesize high-quality UCNPs.

3.1.1. *Hydro(solvo)thermal synthesis method*

In a typical hydrothermal method, reactions occur in a sealed environment under high pressure and temperature, usually above the critical point of the solvent to increase the reactivity and solubility of the inorganic elements. Compared with other types of synthetic methods, hydrothermal method has advantages to implement a set of reactions at the same time and create highly crystalline phase at much lower temperature. A basic hydrothermal method involves a few steps: first, mix rare-earth precursors with fluoride precursors in an aqueous solution, then place them in an autoclave (often Teflon-lined) and finally seal and heat them. The rare-earth precursors usually choose chlorides, nitrates or oxides of rare-earth ions. HF, NH_4F or NH_4HF_2 are universally chosen as the fluoride precursor for synthesis of LnF_3 nanocrystals, and NaF or KF commonly for $MLnF_4$ nanocrystals.[29,30]

With the advantages of high purity and good homogeneity, the solvothermal synthesis method is another important technology for the preparation of UCNPs. Under the same conditions, the solvothermal process can achieve higher air pressure than the hydrothermal process due to its low boiling point, which not only shortens reactant times, but also benefits the crystallinity of products. Additionally, in a solvothermal system, the crystal growth can be controlled and products with different morphologies can be gained.[31–35] Tian *et al.* reported a modified liquid–solid solution solvothermal strategy for synthesizing Mn^{2+}-doped $NaYF_4$:Yb/Er nanoparticles, which possess the rational manipulation of red and green upconversion luminescence, and the pure dark red emission (650–670 nm).[36]

3.1.2. *Thermal decomposition method*

In a typical thermal decomposition procedure, organometallic compounds as precursors are decomposed in a high boiling point organic solvent with the assistance of surfactants at an elevated temperature. The common precursors are lanthanide metal ionic trifluoacetate salts; the solvent can be oleic acid (OA), oleylamine (OM), 1-octadecene (ODE) or trioctylphosphine oxide (TOPO), which can coordinate the metallic elements and the long hydrocarbon chain to prevent nanoparticle aggregation due to their typically functional capping group. Mai *et al.*[37,38] have first developed a general synthetic strategy using the co-thermolysis of the trifluoroacetate precursors in OA/OM/ODE to synthesize fluoride-based nanocrystals. The composition of precursors, reaction time, temperature and coordination property of the solvent played critical roles in controlling the morphology, size, phase and UCL efficiency of the UCNP during the thermolysis process. Xie *et al.*[39] and Wang *et al.*[40] reported the synthesis of monodispersed Nd^{3+}-sensitized core−shell nanoparticles with narrow size distribution and regular morphology using thermal decomposition method. Vetrone *et al.*[41] reported that the nanoparticles coated with a

shell of $NaGdF_4$ could minimize the luminescence quenching caused by the surface defects and surface-associated ligands. They also found that the UCL of the coated nanoparticles was more intense for the core/shell structure. In Cheng *et al.*'s work, the synthesized UCNPs were studied for biological application after modified with different hydrophilic molecules.[42–44] A class of biocompatible UCNPs with largely amplified red-emissions were also developed by Han's group.[45] The quantum yield of red emission reached 3.2, which is 15-fold stronger than the known β-phase core/shell UCNPs. And the red-emission of UCNPs could penetrate a deep-tissue (>1.2 cm) setting *in vivo* at a harmless laser power density. The deeper tumor treatment has been demonstrated by using a UCNP–PDT system. Shi's group successfully fabricated ultrasmall $NaGdF_4$ nanodots (2 nm) with polyethylene glycol (PEG) modification.[46] In their work, DTPA was chelated outside of the UCNPs to capture the potentially released Gd^{3+} ions. The synthesized nanodots were used for atherosclerotic plaque imaging and MR angiography.

3.1.3. *One-pot template-free synthesis*

Recently, hollow UCNPs have attracted crucial attention. Because they not only possess luminescence properties but also provide potential applications in the controlled storage or delivery of therapeutic drugs. Some groups used a template-assisted strategy to synthesize hollow nanoparticles for saving time and energy and allowing rapid production. However, the disadvantages of this strategy, such as low quantum yields and lengthy synthetic procedures and so on, still largely impeded the optimizing production and biomedical application. Alternatively, a template-free process to construct hollow upconversion structures has been developed for simplifying the preparation procedure. In Zhang *et al.*'s work,[47] a facile solution-phase synthesis strategy was used for forming hollow cubic phase α-$NaYF_4$ nanoparticle. They demonstrated that the nanoscale growth of hollow particle with controlled size was induced by the Kirkendall effect. Yang and other researchers also employed the same strategy for synthesizing hollow $NaYF_4$:Yb/Er nanoparticles[48] and core–shell-structured $Yb(OH)CO_3$@$YbPO_4$:Er hollow microspheres.[49] However, in these synthetic scheme, the corresponding oxides or carbonates precursors are still required. To further upgrade the template-free strategy, the Ostwald ripening mechanism was studied and utilized in one-pot synthetic method of Ln-doped luminescent hollow structures. This method not only simplified the synthetic procedure, but also improved the nanoparticles yield.[50] As an example, Li reported an efficient, one-pot route for synthesizing sub-100 nm hydrophilic $NaYF_4$-based upconversion hollow nanospheres in hydrothermal condition.[51]

3.2. *Optimization of UCNPs*

High luminescence efficiency is critical for UCNPs in theranostic application. Three general approaches have been implemented to improve the efficiency (Fig. 2), including (1) selection of efficient host materials; (2) plasmonic enhancement; (3) preparation of core/shell structures.

3.2.1. *Selection of host materials*

Selecting appropriate host materials is essential for high efficiency upconversion emission. Basically, a good host material should have high optical damage threshold, be transparent in the spectral range of interest, and be chemically stable. Up to now, 980 nm excited $NaYF_4$ nanoparticles are the most efficient UCL host. Chen *et al.* reported that the intensity of $NaYF_4$:Yb^{3+}/Tm^{3+} nanocrystal NIR upconversion emission could be tuning, showing 43 times along with an increase in the relative content of Yb^{3+} ions from 20% to 100%, with a corresponding decrease in the Y^{3+} content from 80% to 0%. The synthetic ultrasmall $NaYbF_4$:2% Tm^{3+} nanocrystals displayed 808 nm luminescence

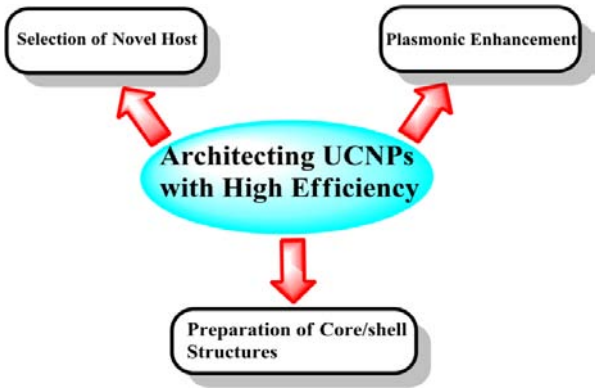

Fig. 2. General strategies to achieve the high efficiency of UCNPs.

emission, which is 3.6 times more intense than $NaYF_4$:20% Yb^{3+}/2% Tm^{3+} nanocrystals.[52]

To obtain UCNPs with different emission and excitation wavelengths, the different doping ions Er^{3+}, Tm^{3+}, Nd^{3+} and Ho^{3+} are frequently used as activators. Yb^{3+} as a sensitizer to enhance the UCL efficiency is often co-doped with Er^{3+}, Tm^{3+} and Ho^{3+}, and it has a larger absorption cross section at around 980 nm than other lanthanide ions. The multicolor luminescent $NaYF_4$:Yb^{3+},Er^{3+} UCNPs was studied by Liu *et al.*[53] Similarly, the Yb^{3+}/Ho^{3+} co-doped UCNP was chemically synthesized and investigated.[54] Nyk *et al.*[55] demonstrated a new approach for photoluminescence imaging *in vitro* and *in vivo* by synthesizing Yb^{3+}, Tm^{3+} co-doped UCNPs. Wang *et al.*[56] reported building a Yb^{3+}, Nd^{3+} co-doped core/shell structure to ensure successive $Nd^{3+} \rightarrow Yb^{3+} \rightarrow$ activator energy transfer. In order to decrease the cross-relaxation energy loss, they used a very low doping percentage of Ln^{3+}(<2 mol%).

3.2.2. *Plasmonic enhancement*

The electromagnetic interaction of the metal with incident light of a specific wavelength can produce localized surface plasmon resonance (LSPR). LSPR can be used to enhance the efficiency of luminescence of UCNPs by setting an appropriate distance between the metallic structure and UCNPs. Through gold nanorod-based LSPR, Zhan *et al.* greatly enhanced UCL. They deposited unconversion materials on the corners of the gold nanorod, the significant overlap provided simultaneous enhancement of excitation and emission.[57] Park *et al.*[58] presented a view of published works on plasmon enhanced upconversion, in regard to the effects of spacer layers and local heating, more detailed discussion on comparable classes of nanostructures, and the dynamics of the plasmon enhanced upconversion process.

3.2.3. *Preparation of core/shell structures*

The fabrication of core/shell architectures is another useful strategy to improve the luminescence of UCNPs. Because a shell with similar lattice constant grown around the UCNPs can reduce nonradiative decay losses of the surface luminescence. Chen *et al.*[24] reported a novel and biocompatible core/shell (α-$NaYbF_4$:Tm^{3+})/CaF_2 nanoparticle, which exhibited highly efficient NIR–NIR upconversion. Through heteroepitaxial growth of a biocompatible CaF_2 shell, the nanopaticle resulted in a 35-fold increase in the intensity of UCL from the core, surface quenching effect. Similarly, a core/shell $NaYbF_4$:Tm^{3+}/$NaGdF_4$ nanoprobe was reported by another group for NIR-to-NIR UCL and magnetic resonance bimodal imaging (MRI).[59] They demonstrated that the coated $NaGdF_4$ shell increased the UCL efficiency of Tm^{3+} ions by about three times. Recently, Zhong group successfully designed a transition layer in the $NaYF_4$:Yb,Er,Nd@$NaYF_4$ core–shell structure to decrease the quenching interaction between Er^{3+} and Nd^{3+} and enhanced the luminescence of 800 nm excited UCNPs.[60] Liu synthesized an core–shell UCNP excited with 795 nm by doping with the high-concentration Nd^{3+} ($\sim$ 20 mol %),[39] markedly increased the UCL efficiency from that with the Er^{3+} or Ho^{3+}.

4. Biological Preparation of UCNPs

4.1. *Surface functionalization of UCNPs*

UCNPs produced by the methods in Sec. 3.1 are often hydrophobic due to the OA, OM, or TOPO molecules capping. To apply UCNPs in biological environment for imaging and therapy, suitable surface properties are required. Modification and functionalization are crucial steps to convert these hydrophobic UCNPs into water-soluble for enhancing the biocompatibility, and provide reactive groups for subsequent bio-conjugation, such as carboxyl ($-$COOH), amino ($-NH_2$) or maleimide (MA) group. To date, common surface-functionalization process including hydrophobic/hydrophobic interaction, ligand exchange, layer-by-layer fabrication, silanization (coating with silica layer) and one-step synthesis of surface functionalized UCNPs have been developed (Fig. 3).[61] Through these methods, $-$COOH, $-NH_2$ or MA groups could be connected to UCNPs and further conjugated with biomolecules, such as folic acid (FA), peptide, protein, DNA and so on.

4.1.1. *Carboxylic acid ($-$COOH) group modification*

The $-$COOH group is particularly easy to react with the biological molecules with $-NH_2$ groups.

Fig. 3. Schematic illustration of general strategies for surface engineering of UCNPs.

Many ligands with carboxyl, such as 4,4-(hexafluoroisopropylidene) diphthalic anhydride (HDA) citrate, polyacrylic acid (PAA), thioglycolic acid (TGA), arachidonic acid (AA), MS methanesulfonic acid (MSA), dimercaptosuccinic acid (DMSA) and diacid PEG could be modified on the UCNPs surface through the surface-functionalization process. Prasad reported that they modified PAA on the surface of the OA-capped UCNPs through a general ligand exchange procedure. Chen *et al.*[62] utilized the Lemieux-von Rudloff reagent to directly oxidize the OA-coated UCNPs for carboxylic acid group generation. Similarly, ozone was also used to directly oxidize the OA ligands on the surface of the UCNPs into ($HOOC(CH_2)_7COOH$) or azelaic aldehyde $HOOC(CH_2)_7CHO$.[63] In Yi and Chow's work, they employed a amphipathic reagent $HOOC–PEG_{600}–COOH$ to decorate the OM-coated $NaYF_4$:Yb,Er nanoparticles for carboxylic group functionalization.[64]

4.1.2. *Amine (–NH_2) group modification*

As carboxylic acid group, amine group can also be modified on UCNPs for conjugation of functional biomolecules with the carboxylic acid group. Hydrophilic ligands, such as poly(amidoamine) (PAMAM), azodicarbonamide (ADA), poly(ethylenimine) (PEI), diamino PEG, para-aminohippuric acid (PAH), could provide $-NH_2$ for the UCNPs surface. The amine densities conjugated on the surface of UCNP could be measured by the 9-fluorenylmethyl chloroformate (FmocCl)[65] or the ninhydrin analysis method.[66] The amine group modified UCNP not only displayed better stability in water solution than the hydrophobic group coated nanoparticles, but also provided the ability to conjugate with FA, biotin, antibody, and DNA that contain $-COOH$ group. In studies, PAH functionalized upconversion hexagonal-phase nanoparticles were connected with biotin as fluorescent probes for bioimaging.[67] PAMAM dendrimers modified $NaGdF_4:Er^{3+}$, Yb^{3+} upconverting nanoparticles (LnNPs) was used for the next molecular connection.[68] In addition, Li reported a novel one-step synthetic strategy for AA-modified UCNPs using a hydrothermal reaction assisted by binary cooperative ligands (HR-BCL).[65] This AA-modified UCNPs could further conjugate with FA for targeting overexpressed folate receptor on tumor cell surface. Another group synthesized PEI capped UCNPs and then used a reactive alkene to connect the PEI.[69] The N-terminal cysteine of the cyclin D-targeting peptide (P_1) thus could react with the alkene to form UCNPs-P_1.

4.1.3. *MA group modification*

MA moiety can react with many sulfydryl group modified biomolecules. MA-functionalized UCNPs generally can be composed of amine modified UCNPs and a functional linker for bio-conjugation. Xiong *et al.* reported the synthesis of MA-functionalized equivalents by using 6-maleimidohexanoic acid N-hydroxysuccinimide ester to modify amine-terminated $NaYF_4$:Yb/Er/Tm UCNPs. Then, the MA–UCNPs were linked with the thiolated cyclopeptide (Arg–Gly–Asp–Phe–Lys(mpa)) for targeted imaging.[67,70] Maeda team[71] structured a MA-functionalized Er-Y_2O_3 by reacting MA–PEG–NHS with APTES–Er–Y_2O_3. So the MA-functionalized UCNPs could be linked with cyclic RGD peptide to specifically target to integrin $\alpha_v\beta_3$ which is highly expressed in the tumor cell surface.

4.2. *UCNPs for tumor targeting in vivo*

Tumor specific targeting of UCNPs plays an key role in tumor diagnosis and treatment. Biological

molecules, including antibodies, FA and peptides, have been used to coat on UCNPs to realize tumor targeting.

4.2.1. *FA-labeled UCNPs*

Many cancer cells can overexpress folate receptors (FR), which are only minimally distributed in normal tissues. Due to the high affinity of FA and FR, FA can be applied as a tumor targeting molecule. Because having nonimmunogenic character, high stability and ability to conjugate with a variety of molecules, FA already has attracted wide attention for tumor targeting of nanoparticles.[72] Xiang and his co-workers first used FA to modify UCNPs for *in vivo* in 2009.[73] Comparing the control group, obvious UCL signals were observed after injection of FA-modified UCNPs into HeLa tumor-bearing nude mouse over a day. Liu *et al.* also reported FA-functionalized $NaYF_4$:Yb^{3+},Er^{3+}–RB nanoconjugates can improve the targeting efficacy in cancer cells for imaging.[53]

4.2.2. *Antibody-labeled UCNPs*

The high affinity interaction of antigen to antibody has become an important strategy of target recognition. Many researchers have reported antibody-modified UCNPs for target delivery and UCL imaging *in vitro*. For example, Jiang *et al.* constructed an anti-Her-2 antibody conjugated UCNP, to be used for interference RNA (siRNA) attaching and delivering to SK-BR-3 cells.[74] However, less reports exhibit that antibody-functionalized UCNPs could successfully target to a specific tumor in animal model.

4.2.3. *Peptide-labeled UCNPs*

Small peptides are usually used to provide tissue penetration and better cellular uptake when introduced to animals. In the research, the arginine-glycineasparatic acid (RGD) peptide plays a pivotal role in tumor targeting, because it has a high affinity to the $\alpha_v\beta_3$ integrin receptor which is highly expressed on tumor cell surface. For example, Zhou *et al.* has successfully constructed a photosensitizer pyropheophorbide a (Ppa) and RGD peptide co-modified $NaYF_4$:Yb/Er upconversion nanoparticle (UCNP–Ppa–RGD) for targeted integrin $\alpha_v\beta_3$-positive U87-MG cells.[75]

5. UCNPs Used as a Theranostic Agent for Tumor Imaging and Therapy

5.1. *UCNPs for tumor optical imaging*

As an excellent optical materials, UCNPs were initially studied for imaging. Compared with the two-photon-absorbed QDs and organic dyes that require expensive pulse laser instrument, UCNPs can use the continuous NIR laser, emitted with an inexpensive diode, as the excitation light. The luminescence is relatively high and stable even at a high fluence rate of irradiation. The capability and feasibility of UCNPs for tumor imaging were demonstrated by many papers: Wu *et al.*[76] reported that UCNPs have photostability, nonblinking and no autofluorescence for cell imaging. Hyeon's group[77] studied the nonbleaching and nonblinking features of UCNPs when it served as an optical imaging nanoprobe. Xiong research team[70] used RGD peptide to conjugate with MA–UCNPs. Their experiments showed that RGD peptide conjugated UCNPs could precisely target U87MG human glioblastoma tumors in mice and realized a vivid bioimaging (Fig. 4).

The great tissue penetration depth of light by use of UCNPs, has also been reported by Wei and others, comparing with the conventional fluoreophores.[61,62,78,79] In Wei's work, the resluts showed that the UCNP had a very stable luminescence in various solution and high tissue penetration deepth with high SNR (Fig. 5). The UCNPs were loaded with the CA4P, an inhibitor of microtube, enhanced the permeability of blood vessel, and thus improved the nanoparticle targeting as well as the UCL imaging.

These studies indicate that UCNPs have many attractive features for imaging. Especially, the proposed imaging technique summarizes several individual properties, such as the deeper tissue penetration depth, the minimized autofluorescence of tissue and the high SNR in one integrated procedure, significantly improved the tumor-imaging capability.

5.2. *UCNPs for multifunctional biomedical imaging*

UCNPs can be used not only for UCL single imaging but also for the multifunctional imaging through combining with some other imaging techniques. The multifunctional lanthanide UCNPs used for UCL/

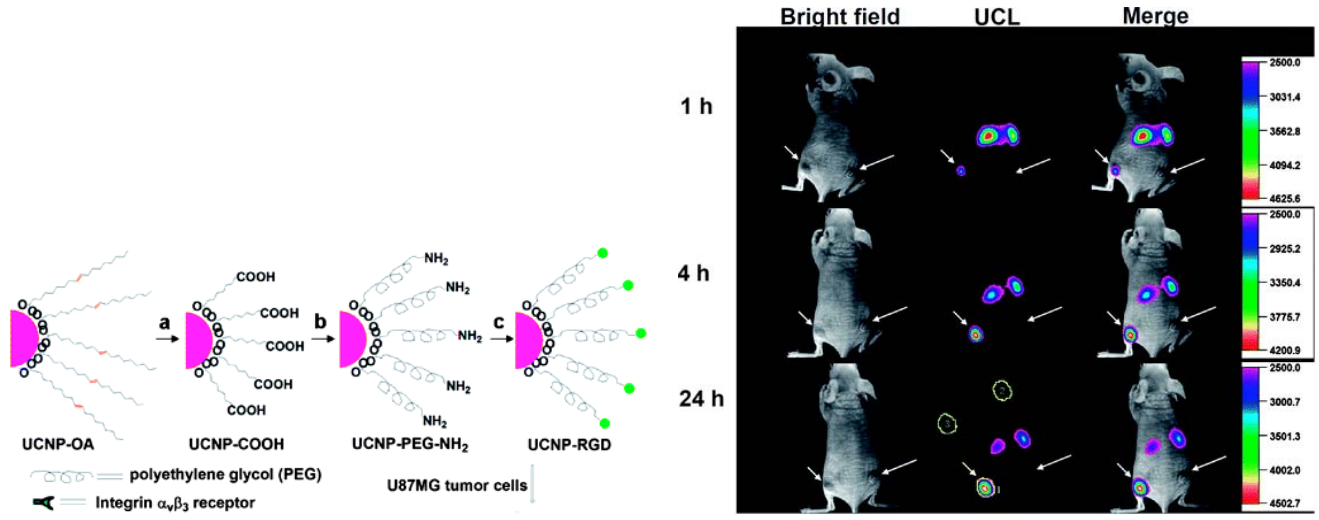

(a) (b)

Fig. 4. *In vivo* tumor-targeted UCL imaging. (a) A scheme showing synthesis of UCNP–RGD. (b) Time-dependent *in vivo* UCL images of a mouse bearing a U87MG tumor (left hind leg, indicated by short arrows) and a MCF-7 tumor (right hind leg, indicated by long arrows) after intravenous injection of UCNP–RGD. (Reprinted with permission from "High contrast UCL targeted imaging *in vivo* using peptide-labeled nanophosphors". Copyright (2009) American Chemical Society.)

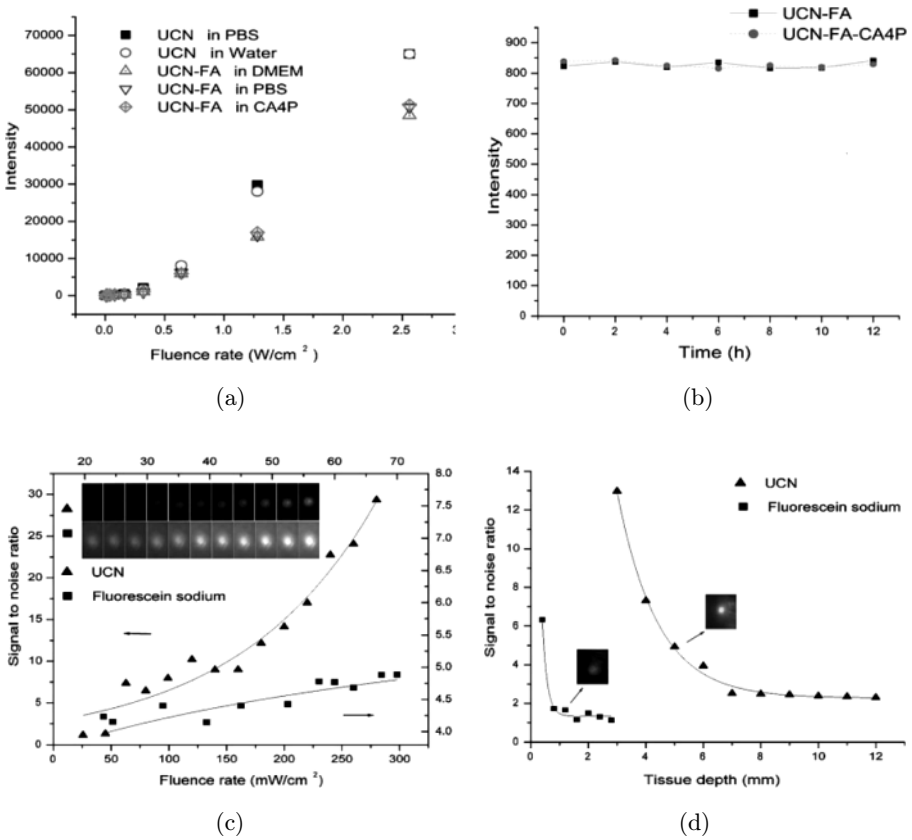

(a) (b) (c) (d)

Fig. 5. (a) The intensity of UCNP–FA dissolved in different aqueous solutions. (b) The anti-photobleaching capability of UCNP–FA. UCNP–FA was irradiated for 12 h continually with a laser (980 nm, 800 mW cm^{-2}). (c) SNR of UCN and fluorescein sodium during laser excitation with different fluence rates. (d) SNR of the UCNPs and fluorescein sodium during laser excitation at different tissue depths. (Reproduced from "High-sensitivity *in vivo* imaging for tumors using a spectral up-conversion nanoparticle $NaYF_4$: Yb^{3+}, Er^{3+} in cooperation with a microtubulin inhibitor" with permission from The Royal Society of Chemistry.)

CT, UCL/MRI and UCL/PET multimodality bioimaging are discussed in this section.

5.2.1. *UCNPs for T_1-weighted and T_2-weighted MRI*

As a most commonly T_1-weighted (Spin-lattice relaxation time) MRI agent, Gd^{3+} has a large paramagnetic moment due to its seven unpaired inner 4f electrons. Some groups used $NaGdF_4$ as a host material to obtain magnetic UCNPs.[59,80–84] For example, Johnson and his co-workers reported a 2.5–8.0 nm $NaGdF_4$:Yb,Er nanoparticle for the T_1-weighted MRI.[80] The Gd^{3+} relaxivity values increased from 3.0 to 7.2 mM^{-1} s^{-1} with decreased particle size. The relaxivity of the 2.5 nm nanoparticles was almost twice than that of the clinical Gd-DTPA (Magnevist). Moreover, $KGdF_4$,[85] Gd_2O_3,[86,87] $GdVO_4$,[22,88] and $GdPO_4$,[89] codoped with Yb^{3+} and Er^{3+} (or Tm^{3+}), were also applied in T_1-weighted MRI.

Another approach with Gd^{3+} for MRI was to dope the ions to the lanthanide UCNPs, such as the fabricated $NaLuF_4$:Gd,Yb,Tm[90] and BaF_2:Yb, Tm@SrF_2:Nd,Gd[91] nanoparticles. Studies showed that Gd^{3+} co-doped nanoprobes could impart strong T_1 and T_2 (spin–spin relaxation time) for high contrast MRI.[92–95]

In addition, directly introducing Gd^{3+}[95] and modifying with gadopentetic acid (Gd-DTPA)[96] onto the UCNP surface were also proposed for T_1-weighted MRI.

T_2-weighted MRI ability of nanostructures mainly rely on combination of UCNPs and superparamagnetic Fe_3O_4 nanoparticles. Shen *et al.* fabricated hetero-nanoparticles composed of Fe_3O_4 and $NaYF_4$:Yb,Er nanophosphors by a crosslinker anchoring process involving DDA or MUA. The magnetic saturation of the resultant hetero-nanoparticles was determined to be 9.25 and 7.05 emu g^{-1}, respectively.[97] Chen and co-workers developed a "neck-formation" method involving silica shielding to combine Fe_3O_4 and $NaYF_4$:Yb,Er nanophosphor into hetero-nanoparticles.[98] The saturation magnetization and r_2 values were measured as 89.8 emu g^{-1} and 211.76 s^{-1} mM^{-1} (3.0 T), respectively.

5.2.2. *UCNPs for positron emission tomography imaging*

By measuring the radioactivity, position emission tomography (PET) imaging has very deep tissue penetration for *in vivo* imaging. ^{18}F is the most widespread radionuclide used in clinical PET imaging, due to its short half-life (110 min). Based on the affinity between Ln^{3+} and F^-, Sun and coworkers had introduced radioactive ^{18}F onto the surface of rare-earth nanoparticles, such as oxide, fluoride and hydroxide.[99] The ^{18}F-labeling process only took 5 min in pure water and the yield of ^{18}F-labeling was more than 90%. The bio-distribution of ^{18}F-labeled rare-earth nanoparticles was further investigated by PET imaging.

5.2.3. *UCNPs for single-photon emission computed tomography imaging*

^{153}Sm as a γ-emitter has been incorporated into single photon emission computed tomography (SPECT) imaging probes used in preclinical and clinical diagnosis. Currently, two methods have been utilized to label lanthanide UCNPs with the radionuclide ^{153}Sm to exhibit the pharmacokinetics of them *in vivo*. One method is to dope ^{153}Sm into Ln^{3+}–UCNPs. Li used a thermal decomposition method.[100,101] and a one-step hydrothermal method[102] to prepare Tm^{3+}, Yb^{3+}, and $^{153}Sm^{3+}$ co-doped $NaLuF_4$ nanoparticles. The obtained radioactive ^{153}Sm-doped $NaLuF_4$:Yb,Tm nanoparticles were accurately tracked by using SPECT imaging. What is more, they have also synthesized radioactive/upconverting $NaLuF_4$:^{153}Sm,Yb,Tm nanoprobes and used them as a blood pool imaging agent for SPECT imaging.[103] The other method is a rare-earth cation-exchange-based postlabeling strategy.[104] The synthesized UCNPs were mainly captured by the mononuclear phagocyte system (liver and spleen). The SPECT imaging was then successfully used for liver and spleen monitoring.

5.2.4. *UCNPs for X-ray computed tomography (CT) imaging*

As is well-known, the higher atomic number and electron density of the computed tomography (CT) agent can have the higher attenuation coefficient. Lanthanide UCNPs have been reported to have higher atomic numbers than iodine, what made them useful as CT contrast agents. He *et al.*[105] reported a novel OA/ionic liquid two-phase system combining the merits of thermal decomposition method and the IL-based strategy to synthesize

high-quality lanthanide-doped $NaGdF_4$ upconversion nanocrystals. The synthesized ultra-small size (~5 nm) $NaGdF_4$:Yb, Er (Ho, Tm) upconversion nanocrystals are effective for dual-mode UCL imaging and CT imaging *in vivo*. Liu and co-workers reported a high contrast Yb-based nanoparticle modified with the biocompatible polymer DSPE-PEG 2000 for X-ray CT imaging.[106] Xing *et al.* used a PEGylated $NaYbF_4$:Tm^{3+} nanopaticles with high X-ray absorption coefficiency for both NIR-fluorescence bioimaging and CT.[107]

Grafting a CT contrast agent onto the UCNPs is another strategy for X-ray CT imaging of lanthanide UCNPs. Suitable small molecules, like Au, or TaO_x nanoparticles, are very popular as the X-ray CT contrast.[108–110] By using β-$NaYF_4$:18% Yb^{3+}, 2% Er^{3+} nanoprobes modified with the contrast, Zhang *et al.* obtained an imaging platform with high visual sensitivity and tissue penetration.[111] The nanoprobes possessed excellent UCL and remarkable CT contrast when the iodine concentration was increased from 0.018 to 0.969 mM.

Besides the above-mentioned imaging technique, multimodality imaging was also recommended for bioimaging to provide a more extensive information and accurate results. For example, Shen *et al.* fabricated a multishell $NaYF_4$:Yb/Tm@$NaLuF_4$@ $NaYF_4$@$NaGdF_4$ nanoprobe for UCL, MRI and CT trimodal imaging. In the study, the core $NaYF_4$:Yb/Tm provided UCL; the first shell $NaLuF_4$ was used to enhance the UCL and to serve as CT contrast; the outermost thin $NaGdF_4$ layer provided the high longitudinal relaxivity (r_1) for MRI; the transition shell of $NaYF_4$ facilitated the formation of $NaGdF_4$ shell and inhibited the energy transfer from inner activator to surface Gd^{3+}.[112]

5.3. *UCNPs for tumor therapy*

UCNPs are not only applied in the field of bioimaging, they are also studied for therapeutic application. For example, photodynamic therapy (PDT) and photothermal therapy (PTT) have studied to utilize UCNPs as the theranostic agents.[75] Through integrating the optical imaging capability and the therapeutical functions, the mulfunctional UCNP has become a powerful weapon for tumor disease fighting.[113,114]

5.3.1. *UCNPs for PDT*

Unlike surgery, chemotherapy and radiotherapy, PDT combines photosensitizer and light source to destruct tumor tissue through photodynamic reaction. Basic elements of PDT include oxygen, photosensitizer and light. Under specific wavelength laser irradiation, the photosensitizer is excited and transfers its energy to the surrounding oxygen to generate reactive oxygen species (ROS). ROS can induce oxidizing reaction with the adjacent biological molecules, thus causing cell damage and death.

However, PDT application is restricted by the limited penetration depth of visible light. The NIR light has a deeper tissue transmission but the photon energy is too low to excite the photosensitizer. Fortunately, UCNPs can do as a medium to receive the NIR light energy and transfer it to photosensitizer molecules for excitation. Thus, the NIR to visible UCNPs possess deep tissue penetration capability and have great superiority to be used in PDT. This capability has been confirmed by Zhou *et al.*[75,115] In Zhou and his co-workers' sequence work, they demonstrated that the UCNP modified with photosensitizer pyropheophorbide-a and RGD peptide could act as a NIR-excited photosensitizer for efficient tumor cell killing and deeper tumor treatment.

To efficiently load photosensitizers and transfer energy, several methods are applied: one method is coating a silica shell on the surface of UCNPs to form a heterogeneous core–shell carrier nanostructures; another is to attaching photosensitizers directly onto the surface of UCNPs through covalent bonding; the third is modifying polymers on the surface of UCNPs for photosensitizer conjugating.

Qian's group[116] utilized mesoporous-silica-coated UCNPs loading a photosensitizer zinc phthalocyanine. The mesoporous silica could protect the photosensitizers from reaction with biological molecules *in vivo*. When the photosensitizers consequently released from the mesoporous silica, singlet oxygen was produced by a NIR laser exciting.

Ungun *et al.*[117] structured a three-layer up-converting nanoprobe which outer layer modified with photosensitizer porphyrin and biocompatible PEG for PDT. In another study, the photosensitizer merocyanine 540 was directly attached on UCNP to be excited by infrared irradiation.[118] The *in vitro* results showed that the UCNPs presented an effective PDT effect on MCF-7/AZ bladder cancer cells.

$NaYF_4$:Yb/Er has also been wrapped with O-carboxymethyl chitosan to connect with the pyropheophorbide-a photosensitizer and the targeting molecule RGD peptide.[63,69,76,115] In this photosensitizer loading method, the constructed nanoparticles successfully presented a significantly deeper therapeutic depth compared with conventional visible light triggered photosensitizer.

With regard to the application of the photosensitizers in UCNP–PDT, besides the above mentioned, some other specific photosensitizers were also studied. Guo *et al.*[119] reported that the photosensitizer of tris-(bipyridine)ruthenium(II) (Ru$(bpy)_3^{2+}$), which has a maximum absorption at 450 nm, was functionalized on silica coated $NaYF_4$:Yb^{3+}/Tm^{3+} nanoparticles. By absorbing the blue emission of Tm^{3+}, $Ru(bpy)_3^{2+}$ could produce $^1O_2$ efficiently; Shan *et al.*[120] reported that the mesotetraphenylporphine photosensitizer excited by the green emission of β-$NaYF_4$:Yb^{3+}/Er^{3+} UCNPs could be used to damage HeLa cells; in Tian *et al.*'s work,[121] photosensitizer chlorine e6 (Ce6), zinc phthalocyanine (ZnPc) and methylene blue (MB) were selected to modify on a specific synthesized red-emitting UCNP for PDT; the photosensitizer ZnPc modified multifunctional UCNPs constructed by Cui *et al.*[122] could inhibit the deep-seated tumor up to 50%; by comparison, the tumor inhibition ratio of the conventional visible light-activated PDT only reached 18% (Fig. 6).

In the most of UCNP–PDT studies, the imaging was simultaneously used to identify the nanoparticles localization for more precise tumor treatment purpose.[76,115,123–128] They used photosensitizer for PDT, and UCL or other imaging method for particle/tumor localization. The integration improves the treatment effects and gives a promising biomedicine application strategy.

5.3.2. *UCNPs for PTT*

PTT uses a NIR light to excite photoabsorbers and then generates heat to damage cancer cells. Many groups have paid close attention to study PTT as a cancer therapies. Since UCNPs have its advantages

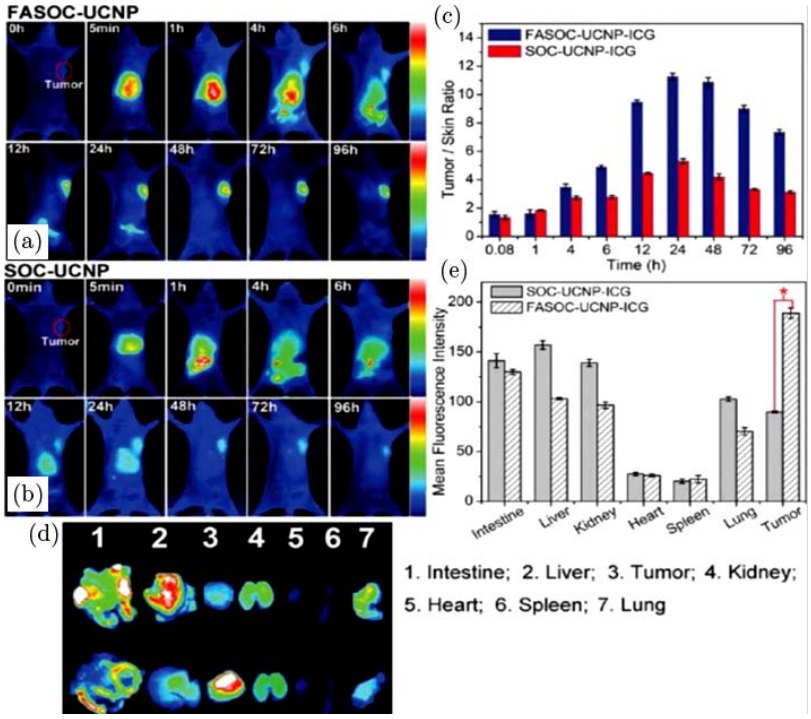

Fig. 6. *In vivo* tumor-targeting of the nanoconstructs. Fluorescence images of nude mice bearing Bel-7402 tumors with intravenously injection of (a) FASOC–UCNP–ICG and (b) SOC–UCNP–ICG; (c) tumor/skin ratio of tumor-bearing mice injected with different nanoconstructs; (d) fluorescence images of isolated organs separated from Bel-7402 tumor-bearing mice in different groups at 24 h postinjection; (e) semiquantification of FASOC–UCNP–ICG and SOC–UCNP–ICG in the isolated organs of mice with different injection. (Reprinted with permission from "*in vivo* targeted deep-tissue photodynamic therapy based near-infrared light triggered upconversion nanoconstruct". Copyright (2013) American Chemical Society.)

on optical imaging and the optical absorbers loading, they have been studied for uses in PTT applications.

Dong *et al.*[129] synthesized a core–shell $NaYF_4$:Yb^{3+},Er^{3+}@Ag nanoparticles with unique biofunctional specialty for imaging and tumor eradication. They observed the significantly photothermal induced death in both human hepatic cancer cells HepG2 and breast cancer cells BCap-37, which were incubated with the composite NPs *in vitro* and under 980 nm NIR excitation.

Additionally, by decorating ultra-small plasmonic CuS nanoparticles onto the surface of silica-coated UCNPs, another group[130] constructed a novel multifunctional core/satellite nanotheranostic (CSNT) for integrated *in vivo* imaging and tumor treatment. These CSNTs could perform PTT thermal ablation and implement highly localized radiation dose to increase the radiation therapy efficiency both *in vitro* and *in vivo* (Fig. 7). The tumor could be entirely eliminated in 120 days under the associated interaction between photothermal absorption and the enhanced radiotherapy. Notably, the CSNTs showed nontoxic for the mice within a month. Through layer-by-layer self-assembly method, Cheng *et al.*[108] created Fe_3O_4 coated $NaYF_4$:Yb^{3+}/Er^{3+} UCNPs, on top of which a thin gold shell was formed by seed-induced reduction growth. The photothermal cancer treatment mainly owed to the gold shell, which possess the surface plasmon resonance absorption.

5.3.3. *UCNPs for chemotherapy*

Similar to the application in PTT, UCNPs were used for chemotherapy. In the reported protocols,

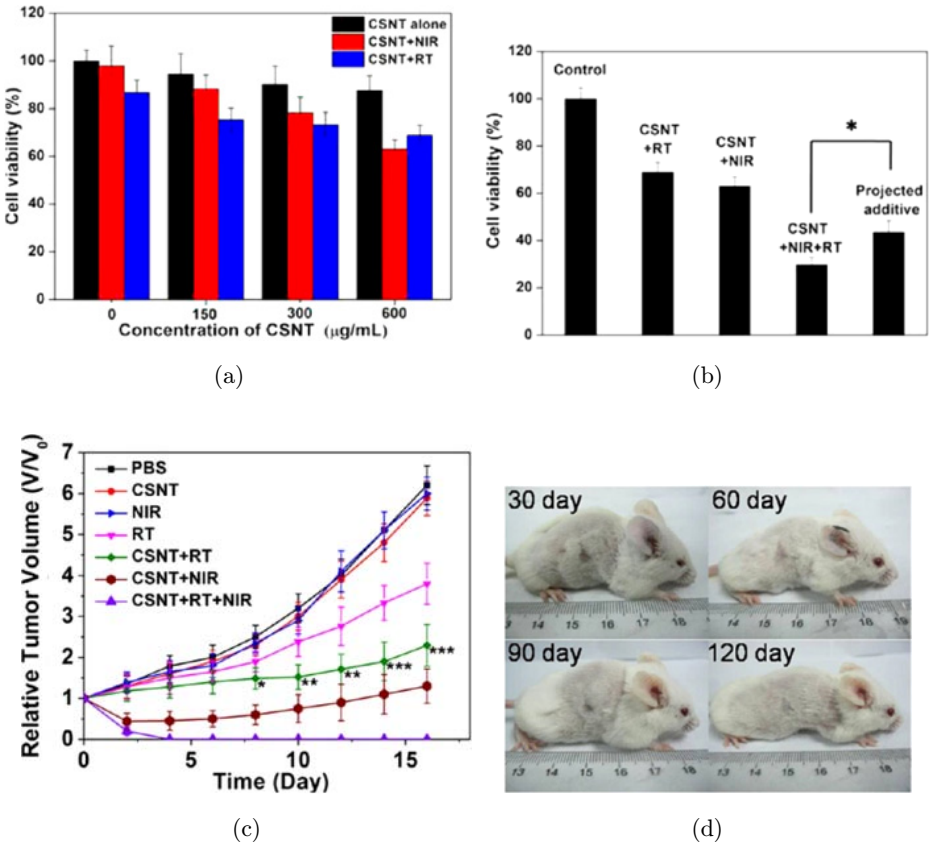

(a) (b) (c) (d)

Fig. 7. (a) Quantitative analysis of the cell viability with CSNTs at varied concentrations with or without NIR-laser irradiation and RT. (b) Synergistic therapeutic effect of Hela cells that have taken up CSNTs subjected to RT, PTA, and the combined RT/PTA treatments. (c) Time-dependent tumor growth curves of different groups of mice with various treatments. In all experiments, the power density of 980 nm NIR-laser and the radiation dose used for RT were kept constant at 1.5 W/cm^2 and 6 Gy, respectively. (d) The photographs of mice in 30, 60, 90, and 120 days of treatment (group 7) showing the complete eradication of the tumor and no visible recurrences of the tumors in at least 120 days. (Reprinted with permission from "A core/satellite multifunctional nanotheranostic for *in vivo* imaging and tumor eradication by radiation/photothermal synergistic therapy". Copyright (2013) American Chemical Society.)

UCL was utilized for chemo drug monitoring, including the distribution, localization, aggregation, and so on. To build up UCNP-based systems for drug delivery, mesoporous silica shells, hydrophobic pockets, and hollow spheres with mesoporous surface were studied. Xu *et al.*[131] projected an UC-IO@Polymer multi-functional nanocomposite system by encapsulating hydrophobic UCNP together with iron oxide nanoparticles into the copolymer poly(styrene-block-allyl alcohol) (PS_{16}-b-PAA_{10}). Doxorubicin was loaded into the UC-IO@Polymer to form UC-IO@Polymer-DOX complex for imaging-guided and magnetic-targeted drug delivery. Recently, Hou's group synthesized porous $NaYF_4$:Yb,Er@silica fiber,[132] Gd_2O_3:Er@nSiO_2@mSiO_2 nanocomposite[133] and $Yb(OH)CO_3$@$YbPO_4$:Er hollow spheres[49] as the drug carriers. They demonstrated that the UCL could sensitively be used for monitoring and tracking the drug release.

Nitric oxide (NO) shows great potential for antirestenosis, anticancer and antibacterial. Therefore, successful NO-delivery is becoming one important issue in the biomedical application of NO. UCNPs have been successfully designed as a NIR sensitized system for NO carrying and therapy.[134–136] In these studies, Roussin's black salt (RBS) was used as the NO yielding source. UCNPs coated with SiO_2/-NH^{3+}, poly (dimethylsiloxane) composites, mSiO_2 were used for RBS carrying and photo-triggered releasing for cancer therapy.

5.3.4. *UCNPs for gene therapy*

Gene therapy is the therapeutic delivery of nucleic acid polymers into a patient's cells to treat disease. RNA interference (RNAi) often is used in gene therapy, and represents a powerful, naturally occurring biological strategy for inhibition of gene expression. It is mediated through small interfering RNAs (siRNAs), which trigger specific mRNA degradation. The success of gene therapy is largely dependent on the development of the gene delivery vector. Utilizing UCNPs as gene carriers can simultaneously realize the gene delivery and its monitoring. Many studies have implemented this application of UCNPs. Jiang *et al.*[74] reported that FA and anti-Her2 antibody were successfully conjugated with UCNPs for targeted delivery of siRNA and cell imaging. $NaYF_4$:Yb, Er was also employed as a carrier for BOBO-3-stained siRNAs delivery.[137] The UCNPs transferred its energy to the BOBO-3 fluorescent acceptor through fluorescence resonance energy transfer (FRET) mechanism. Release of siRNA in cells gradually persisted for 24 h via intracellular FRET analysis. Recently, Jaya Kumar and co-workers developed a novel method to encapsulate photocaged DNA/siRNA molecules into the porous silica shell of the mesoporous silica-coated $NaYF_4$:Yb/Tm UCNPs for remotely controlling gene expression.[138] The nanostructures not only increased the payload capacity, but also improved biocompatibility, offered a more efficient loading and delivery of the DNA/siRNA. Under NIR excitation, these photocaged plasmid DNA or siRNA could be activated by the UV light emitted from UCNPs and then induce expression or downregulation of the specific gene. The utilization of UCNPs co improved the depth of light penetration and the efficiency of the therapy.

6. Toxicity of UCNPs

The *in vitro* cytotoxicity and long-term living toxicity of UCNPs have been investigated by many researchers. In the process, MTS, MTT, CCK-8 and mitochondrial metabolic activity assays[139] were used. The results show that the fabricated UCNPs had a low cytotoxicity in the employed incubation time and drug concentration. The long-term living toxicity of UCNPs has also been evaluated by several proposed methods, such as the serum biochemistry assays, body weight measurement, histology and hematology analysis, behavior observation, and so on. Jalil and Zhang[140] has controlled the dose of silica-coated $NaYF_4$:Yb,Er nanoparticles at 10 mg kg^{-1} in body of rats and no toxic effect was observed via body weight measurement. Through behavior observation, another group[141] reported that mice, which were injected $NaGdF_4$:Yb,Er,Tm nanoparticles, did not show abnormal behavior and could survive for more than one month.

Although all the experiments have shown a low toxicity in biomedical application, it is agreed by researches that further studies on toxicity of UCNPs are still necessary. More detailed investigation about the biomedical security should be conducted in the future work, especially on the long-term organ toxicity.

7. Challenges and Future Opportunities of UCNPs in Tumor Application

In clinical procedure, theranostic agent is consumingly required. The unique character and advantages of UCNPs could not only greatly benefit the biomedical application but also showed encouraged results in PDT, PTT and chemotherapy application. As a promising theranositc agent, UCNP can work as efficient drug nanocarrier and sensitive optical indicator. In the future, UCNP would be well developed and their bio-application would be greatly improved. We believe that some important details in synthesis utility of the promising nanoparticles should be concerned in current. They can be concluded as below:

(1) To obtain the ultra-small, surface-hydrophilic and biocompatible high efficient UCNPs, exploring new synthetic method and surface-modification process is still necessary. Uniforming growth rate of the crystal and reducing the crystal defects of UCNP are also important.
(2) The surface ligand of UCNPs is important for the biological stability and the UCL efficiency. The coordination ability, reaction activity, and stability of UCNPs all refer to the surface properties including zeta potential, functional groups and so on. Hence, further exploration of the surface chemistry of UCNPs is demanded.
(3) For high contrast imaging, a multifunctional nanoprobe should have the optimized radioactive, magnetic and optical properties. Although researchers have obtained some successful results, multimodal imaging based on multifunctional UCNPs, especially the targeting UCNPs, still need to be developed.
(4) Combining UCNP-based PDT or PTT with the guidance of UCL-based imaging has a great perspective to achieve more effective therapeutic effect *in vitro* and *in vivo*. But more efficient imaging-guided therapy which integrates drug delivery monitoring, tumor localization, optical therapy and treatment effect monitoring in a UCNP nanoplatform still need to be further investigated.
(5) Although a low cytotoxicity of the UCNPs has been demonstrated, further nanotoxicology and pharmacokinetics studies, including the dynamics of drug absorption, distribution, metabolism, elimation to the UCNPs with different shapes, sizes and surface coatings should be carefully confirmed.

8. Conclusions

In this review, we have described the recent developments of UCNPs in the design, synthesis and application in bioimaging and therapy. UCNPs have been recognized as a technological marvel with excellent optical properties including non-photobleaching, nonblinking, low-toxicity, no autofluorescence interference and deep tissue penetration synthesis and application. As an effective tumor imaging and therapy nanoagent, it gives a promising future for biomedical application.

Acknowledgments

This research is supported by the National Natural Science Foundation of China (91539127; 61361160414), the Guangdong Natural Science Foundation (2015A030313394), and the Science and Technology Planning Project (2014A020212738) of Guangdong Province, China.

References

1. B. N. Giepmans, S. R. Adams, M. H. Ellisman, R. Y. Tsien, "The fluorescent toolbox for assessing protein location and function," *Science* **312**, 217–224 (2006).
2. T. Terai, T. Nagano, Fluorescent probes for bioimaging applications, *Current Opin. Chem. Biol.* **12**, 515–521 (2008).
3. M. Beija, C. A. Afonso, J. M. Martinho, "Synthesis and applications of rhodamine derivatives as fluorescent probes," *Chem. Soc. Rev.* **38**, 2410–2433 (2009).
4. S. V. Eliseeva, J.-C. G. Bünzli, "Lanthanide luminescence for functional materials and bio-sciences," *Chem. Soc. Rev.* **39**, 189–227 (2010).
5. H. Liu, F. Zhan, F. Liu, M. Zhu, X. Zhou, D. Xing, "Visual and sensitive detection of viable pathogenic bacteria by sensing of RNA markers in gold nanoparticles based paper platform," *Biosens. Bioelectron.* **62**, 38–46 (2014).
6. X. Michalet, F. F. Pinaud, L. A. Bentolila, J. M. Tsay, S. Doose, J. J. Li *et al.*, "Quantum dots for live cells, *in vivo* imaging, and diagnostics," *Science* **307**, 538–544 (2005).

7. Y. Liao, X. Zhou, D. Xing, "Quantum dots and graphene oxide fluorescent switch based multivariate testing strategy for reliable detection of listeria monocytogenes," *ACS Appl. Mater. Interfaces* **6**, 9988–9996 (2014).
8. Y. Liu, D. Tu, H. Zhu, E. Ma, X. Chen, "Lanthanide-doped luminescent nano-bioprobes: From fundamentals to biodetection," *Nanoscale* **5**, 1369–1384 (2013).
9. D. Peer, J. M. Karp, S. Hong, O. C. Farokhzad, R. Margalit, R. Langer, "Nanocarriers as an emerging platform for cancer therapy," *Nat. Nanotechnol.* **2**, 751–760 (2007).
10. L. Wen, W. Ding, S. Yang, D. Xing, "Microwave pumped high-efficient thermoacoustic tumor therapy with single wall carbon nanotubes," *Biomaterials* **75**, 163–173 (2016).
11. H. Qin, T. Zhou, S. Yang, D. Xing, "Fluorescence quenching nanoprobes dedicated to *in vivo* photoacoustic imaging and high-efficient tumor therapy in deep-seated tissue," *Small* **11**, 2675–2686 (2015).
12. H. W. Leverenz, F. Urbach, "Introduction to the Luminescence of Solids," *Phys. Today* **3**, 32–33 (2009).
13. F. Auzel, "Compteur quantique par transfert denergie entre deux ions de terres rares dans un tungstate mixte ET dans un verre," *C. R. Hebd. Seances Acad. Sci. B* **262**, 1016 (1966).
14. T. Forster, *Naturwiss* **33**, 166 (1946), *Ann. Phys.* **2**, 55 (1948).
15. D. L. Dexter, "A theory of sensitized luminescence in solids," *J. Chem. Phys.* **21**, 836–850 (1953).
16. F. E. Auzel, "Materials and devices using double-pumped-phosphors with energy transfer," *Proc. IEEE* **61**, 758–786 (1973).
17. V. Ovsyankin, P. Feofilov, "Cooperative optical phenomena in condensed media," *Phys.-Usp.* **15**, 354 (1972).
18. E. Nakazawa, S. Shionoya, "Cooperative luminescence in $YbPO_4$," *Phys. Rev. Lett.* **25**, 1710 (1970).
19. J. S. Chivian, W. Case, D. Eden, "The photon avalanche: A new phenomenon in Pr^{3+}-based infrared quantum counters," *Appl. Phys. Lett.* **35**, 124–125 (1979).
20. S. Sivakumar, P. R. Diamente, F. C. van Veggel, "Silica-coated Ln^{3+}-doped LaF_3 nanoparticles as robust down-and upconverting biolabels," *Chemistr* **12**, 5878–5884 (2006).
21. H. Guo, N. Dong, M. Yin, W. Zhang, L. Lou, S. Xia, "Visible upconversion in rare earth ion-doped Gd_2O_3 nanocrystals," *J. Phys. Chem. B* **108**, 19205–19209 (2004).
22. W. Yin, L. Zhou, Z. Gu, G. Tian, S. Jin, L. Yan *et al.*, "Lanthanide-doped $GdVO_4$ upconversion nanophosphors with tunable emissions and their applications for biomedical imaging," *J. Mater. Chem.* **22**, 6974–6981 (2012).
23. F. Evanics, P. Diamente, F. Van Veggel, G. Stanisz, R. Prosser, "Water-soluble GdF_3 and GdF_3/LaF_3 nanoparticles physical characterization and NMR relaxation properties," *Chem. Mater.* **18**, 2499–2505 (2006).
24. G. Chen, J. Shen, T. Y. Ohulchanskyy, N. J. Patel, A. Kutikov, Z. Li *et al.*, "(α-NaYbF4:Tm^{3+})/CaF_2 core/shell nanoparticles with efficient near-infrared to near-infrared upconversion for high-contrast deep tissue bioimaging," *ACS Nano* **6**, 8280–8287 (2012).
25. F. Vetrone, J.-C. Boyer, J. A. Capobianco, A. Speghini, M. Bettinelli, "Significance of Yb^{3+} concentration on the upconversion mechanisms in codoped Y_2O_3: Er^{3+}, Yb^{3+} nanocrystals," *J. Appl. Phys.* **96**, 661–667 (2004).
26. G. Chen, Y. Zhang, G. Somesfalean, Z. Zhang, Q. Sun, F. Wang, "Two-color upconversion in rare-earth-ion-doped ZrO_2 nanocrystals," *Appl. Phys. Lett.* **89**, 3105 (2006).
27. X. Luo, W. Cao, "Blue, green, red upconversion luminescence and optical characteristics of rare earth doped rare earth oxide and oxysulfide," *Sci. China Ser. B: Chem.* **50**, 505–513 (2007).
28. Y. Sun, H. Liu, X. Wang, X. Kong, H. Zhang, "Optical spectroscopy and visible upconversion studies of YVO_4: Er^{3+} nanocrystals synthesized by a hydrothermal process," *Chem. Mater.* **18**, 2726–2732 (2006).
29. J. Liu, N. Li, R. Wu, Y. Zhao, Q. Zhan, S. He, "Sub-5-nm lanthanide-doped ZrO_2@$NaYF_4$ nanodots as efficient upconverting probes for rapid scanning microscopy and aptamer-mediated bioimaging," *Opt. Mater. Express* **5**, 1759–1771 (2015).
30. M. Wang, C.-C. Mi, W.-X. Wang, C.-H. Liu, Y.-F. Wu, Z.-R. Xu *et al.*, "Immunolabeling ans NIR-excited fluorescent imaging of HeLa cells by using $NaYF_4$: Yb, Er upconversion nanoparticles," *Acs Nano* **3**, 1580–1586 (2009).
31. B. Tang, J. Ge, C. Wu, L. Zhuo, J. Niu, Z. Chen *et al.*, "Sol–solvothermal synthesis and microwave evolution of $La(OH)_3$ nanorods to La_2O_3 nanorods," *Nanotechnology* **15**, 1273 (2004).
32. R. I. Walton, "Subcritical solvothermal synthesis of condensed inorganic materials," *Chem. Soc. Rev.* **31**, 230–238 (2002).
33. Z. Chen, Q. Tian, Y. Song, J. Yang, J. Hu, "PEG-mediated solvothermal synthesis of $NaYF_4$: Yb/Er superstructures with efficient upconversion luminescence," *J. Alloys Comp.* **506**, L17–L21 (2010).

34. T. He, W. Wei, L. Ma, R. Chen, S. Wu, H. Zhang *et al.*, "Mechanism studies on the superior optical limiting observed in graphene oxide covalently functionalized with upconversion $NaYF_4$:Yb^{3+}/Er^{3+} nanoparticles," *Small* **8**, 2163–2168 (2012).
35. Z. Li, Y. Zhang, "An efficient and user-friendly method for the synthesis of hexagonal-phase $NaYF_4$: Yb, Er/Tm nanocrystals with controllable shape and upconversion fluorescence," *Nanotechnology* **19**, 345606 (2008).
36. G. Tian, Z. Gu, L. Zhou, W. Yin, X. Liu, L. Yan *et al.*, "Mn^{2+} Dopant-controlled synthesis of $NaYF_4$: Yb/Er upconversion nanoparticles for *in vivo* imaging and drug delivery," *Adv. Mater.* **24**, 1226–1231 (2012).
37. H.-X. Mai, Y.-W. Zhang, L.-D. Sun, C.-H. Yan, "Highly efficient multicolor up-conversion emissions and their mechanisms of monodisperse $NaYF_4$: Yb, Er core and core/shell-structured nanocrystals," *J. Phys. Chem. C* **111**, 13721–13729 (2007).
38. H.-X. Mai, Y.-W. Zhang, R. Si, Z.-G. Yan, L.-d. Sun, L.-P. You *et al.*, "High-quality sodium rare-earth fluoride nanocrystals: controlled synthesis and optical properties," *J. Am. Chem. Soc.* **128**, 6426–6436 (2006).
39. X. Xie, N. Gao, R. Deng, Q. Sun, Q.-H. Xu, X. Liu, "Mechanistic investigation of photon upconversion in Nd^{3+}-sensitized core-shell nanoparticles," *J. Am. Chem. Soc.* **135**, 12608–12611 (2013).
40. F. Wang, R. Deng, X. Liu, "Preparation of core-shell $NaGdF_4$ nanoparticles doped with luminescent lanthanide ions to be used as upconversion-based probes," *Nat. Protoc.* **9**, 1634–1644 (2014).
41. F. Vetrone, R. Naccache, V. Mahalingam, C. G. Morgan, J. A. Capobianco, "The active-core/active-shell approach: A strategy to enhance the upconversion luminescence in lanthanide-doped nanoparticles," *Adv. Funct. Mater.* **19**, 2924–2929 (2009).
42. L. Cheng, K. Yang, Y. Li, X. Zeng, M. Shao, S.-T. Lee *et al.*, "Multifunctional nanoparticles for upconversion luminescence/MR multimodal imaging and magnetically targeted photothermal therapy," *Biomaterials* **33**, 2215–2222 (2012).
43. L. Cheng, K. Yang, M. Shao, S.-T. Lee, Z. Liu, "Multicolor *in vivo* imaging of upconversion nanoparticles with emissions tuned by luminescence resonance energy transfer," *J. Phys. Chem. C* **115**, 2686–2692 (2011).
44. L. Cheng, K. Yang, S. Zhang, M. Shao, S. Lee, Z. Liu, "Highly-sensitive multiplexed *in vivo* imaging using PEGylated upconversion nanoparticles," *Nano Res.* **3**, 722–732 (2010).
45. A. Punjabi, X. Wu, A. Tokatli-Apollon, M. El-Rifai, H. Lee, Y. Zhang *et al.*, "Amplifying the red-emission of upconverting nanoparticles for biocompatible clinically used prodrug-induced photodynamic therapy," *ACS Nano* **8**, 10621–10630 (2014).
46. H. Xing, S. Zhang, W. Bu, X. Zheng, L. Wang, Q. Xiao *et al.*, "Ultrasmall NaGdF4 nanodots for efficient MR angiography and atherosclerotic plaque imaging," *Adv. Mater.* **26**, 3867–3872 (2014).
47. F. Zhang, Y. Shi, X. Sun, D. Zhao, G. D. Stucky, "Formation of hollow upconversion rare-earth fluoride nanospheres: Nanoscale kirkendall effect during ion exchange," *Chem. Mater.* **21**, 5237–5243 (2009).
48. D. Yang, X. Kang, Y. Dai, Z. Hou, Z. Cheng, C. Li *et al.*, "Hollow structured upconversion luminescent $NaYF_4$: Yb^{3+}, Er^{3+} nanospheres for cell imaging and targeted anti-cancer drug delivery," *Biomaterials* **34**, 1601–1612 (2013).
49. Z. Xu, Ma Pa, C. Li, Z. Hou, X. Zhai, S. Huang *et al.*, "Monodisperse core-shell structured upconversion $Yb(OH)CO_3$@$YbPO_4$:Er^{3+} hollow spheres as drug carriers," *Biomaterials* **32**, 4161–4173 (2011).
50. M. K. Devaraju, S. Yin, T. Sato, "A fast and template free synthesis of Tb:Y_2O_3 hollow microspheres via supercritical solvothermal method," *Cryst. Growth Des.* **9**, 2944–2949 (2009).
51. G. Tian, L. Duan, X. Zhang, W. Yin, L. Yan, L. Zhou *et al.*, "One-pot template-free synthesis of $NaYF_4$ upconversion hollow nanospheres for bioimaging and drug delivery," *Chem.* **9**, 1655–1662 (2014).
52. G. Chen, T. Y. Ohulchanskyy, R. Kumar, H. Ågren, P. N. Prasad, "Ultrasmall monodisperse $NaYF_4$:Yb^{3+}/Tm^{3+} nanocrystals with enhanced near-infrared to near-infrared upconversion photoluminescence," *ACS Nano* **4**, 3163–3168 (2010).
53. K. Liu, X. Liu, Q. Zeng, Y. Zhang, L. Tu, T. Liu *et al.*, "Covalently assembled NIR nanoplatform for simultaneous fluorescence imaging and photodynamic therapy of cancer cells," *ACS Nano* **6**, 4054–4062 (2012).
54. G.-S. Yi, G.-M. Chow, "Colloidal LaF_3:Yb, Er, LaF_3:Yb, Ho and LaF_3:Yb, Tm nanocrystals with multicolor upconversion fluorescence," *J. Mater. Chem.* **15**, 4460–4464 (2005).
55. M. Nyk, R. Kumar, T. Y. Ohulchanskyy, E. J. Bergey, P. N. Prasad, "High contrast *in vitro* and *in vivo* photoluminescence bioimaging using near infrared to near infrared up-conversion in $Tm^{3+}$and Yb^{3+} doped fluoride nanophosphors," *Nano Lett.* **8**, 3834–3838 (2008).

56. Y.-F. Wang, G.-Y. Liu, L.-D. Sun, J.-W. Xiao, J.-C. Zhou, C.-H. Yan, "Nd^{3+}-sensitized upconversion nanophosphors: Efficient *in vivo* bioimaging probes with minimized heating effect," *ACS Nano* **7**, 7200–7206 (2013).
57. Q. Zhan, X. Zhang, Y. Zhao, J. Liu, S. He, "Tens of thousands-fold upconversion luminescence enhancement induced by a single gold nanorod," *Laser Photonics Rev.* **9**, 479–487 (2015).
58. W. Park, D. Lu, S. Ahn, "Plasmon enhancement of luminescence upconversion," *Chem. Soc. Rev.* **44**, 2940–2962 (2015).
59. G. Chen, T. Y. Ohulchanskyy, W. C. Law, H. Ågren, P. N. Prasad, "Monodisperse $NaYbF_4$: Tm^{3+}/$NaGdF_4$ core/shell nanocrystals with near-infrared to near-infrared upconversion photoluminescence and magnetic resonance properties," *Nanoscale* **3**, 2003–2008 (2011).
60. Y. Zhong, G. Tian, Z. Gu, Y. Yang, L. Gu, Y. Zhao *et al.*, "Elimination of photon quenching by a transition layer to fabricate a quenching-shield sandwich structure for 800 nm excited upconversion luminescence of Nd^{3+}-sensitized nanoparticles," *Adv. Mater.* **26**, 2831–2837 (2014).
61. G. Chen, H. Qiu, P. N. Prasad, X. Chen, "Upconversion nanoparticles: Design, nanochemistry, and applications in theranostics," *Chem. Rev.* **114**, 5161–5214 (2014).
62. Z. Chen, H. Chen, H. Hu, M. Yu, F. Li, Q. Zhang *et al.*, "Versatile synthesis strategy for carboxylic acid-functionalized upconverting nanophosphors as biological labels," *J. Am. Chem. Soc.* **130**, 3023–3029 (2008).
63. H. P. Zhou, C. H. Xu, W. Sun, C. H. Yan, "Clean and flexible modification strategy for carboxyl/aldehyde-functionalized upconversion nanoparticles and their optical applications," *Adv. Funct. Mater.* **19**, 3892–3900 (2009).
64. G. S. Yi, G. M. Chow, "Synthesis of hexagonal-phase $NaYF_4$:Yb, Er and $NaYF_4$:Yb, Tm nanocrystals with efficient up-conversion fluorescence," *Adv. Funct. Mater.* **16**, 2324–2329 (2006).
65. T. Cao, Y. Yang, Y. Gao, J. Zhou, Z. Li, F. Li, "High-quality water-soluble and surface-functionalized upconversion nanocrystals as luminescent probes for bioimaging," *Biomaterials* **32**, 2959–2968 (2011).
66. J. Zhou, L. Yao, C. Li, F. Li, "A versatile fabrication of upconversion nanophosphors with functional-surface tunable ligands," *J. Mater. Chem.* **20**, 8078–8085 (2010).
67. L. Wang, R. Yan, Z. Huo, L. Wang, J. Zeng, J. Bao *et al.*, "Fluorescence resonant energy transfer biosensor based on upconversion-luminescent nanoparticles," *Angew. Chem. Int. Ed. Engl.* **44**, 6054–6057 (2005).
68. N. Bogdan, F. Vetrone, R. Roy, J. A. Capobianco, "Carbohydrate-coated lanthanide-doped upconverting nanoparticles for lectin recognition," *J. Mater. Chem.* **20**, 7543–7550 (2010).
69. C.-F. Chan, M.-K. Tsang, H. Li, R. Lan, F. L. Chadbourne, W.-L. Chan *et al.*, "Bifunctional upconverting lanthanide nanoparticles for selective *in vitro* imaging and inhibition of cyclin D as anticancer agents," *J. Mater. Chem. B* **2**, 84–91 (2014).
70. L. Xiong, Z. Chen, Q. Tian, T. Cao, C. Xu, F. Li, "High contrast upconversion luminescence targeted imaging *in vivo* using peptide-labeled nanophosphors," *Anal. Chem.* **81**, 8687–8694 (2009).
71. T. Zako, H. Nagata, N. Terada, A. Utsumi, M. Sakono, M. Yohda *et al.*, "Cyclic RGD peptide-labeled upconversion nanophosphors for tumor cell-targeted imaging," *Biochem. Biophys. Res. Commun.* **381**, 545–548 (2009).
72. J. Zhong, L. Wen, S. Yang, L. Xiang, Q. Chen, D. Xing, "Imaging-guided high-efficient photoacoustic tumor therapy with targeting gold nanorods," *Nanomedicine* (2015).
73. L.-Q. Xiong, Z.-G. Chen, M.-X. Yu, F.-Y. Li, C. Liu, C.-H. Huang, "Synthesis, characterization, and *in vivo* targeted imaging of amine-functionalized rare-earth up-converting nanophosphors," *Biomaterials* **30**, 5592–5600 (2009).
74. S. Jiang, Y. Zhang, K. M. Lim, E. K. Sim, L. Ye, "NIR-to-visible upconversion nanoparticles for fluorescent labeling and targeted delivery of siRNA," *Nanomedicine* **11**, 1499–1509 (2015).
75. A. Zhou, Y. Wei, B. Wu, Q. Chen, D. Xing, "Pyropheophorbide A and c(RGDyK) comodified chitosan-wrapped upconversion nanoparticle for targeted near-infrared photodynamic therapy," *Mol. Pharm.* **9**, 1580–1589 (2012).
76. S. Wu, G. Han, D. J. Milliron, S. Aloni, V. Altoe, D. V. Talapin *et al.*, "Non-blinking and photostable upconverted luminescence from single lanthanide-doped nanocrystals," *Proc. Nat. Acad. Sci.* **106**, 10917–10921 (2009).
77. Y. I. Park, J. H. Kim, K. T. Lee, K.-S. Jeon, H. B. Na, J. H. Yu *et al.*, "Nonblinking and nonbleaching upconverting nanoparticles as an optical imaging nanoprobe and T_1 magnetic resonance imaging contrast agent," *Adv. Mater.* **21**, 4467 (2009).
78. Y. Wei, Q. Chen, B. Wu, A. Zhou, D. Xing, "High-sensitivity *in vivo* imaging for tumors using a spectral up-conversion nanoparticle $NaYF_4$: Yb^{3+}, Er^{3+} in cooperation with a microtubulin inhibitor," *Nanoscale* **4**, 3901–3909 (2012).

79. J. Liu, R. Wu, N. Li, X. Zhang, Q. Zhan, S. He, "Deep, high contrast microscopic cell imaging using three-photon luminescence of β-($NaYF_4$: Er^{3+}/$NaYF_4$) nanoprobe excited by 1480-nm CW laser of only 1.5-mW," *Biomed. Opt. Express* **6**, 1857–1866 (2015).
80. N. J. Johnson, W. Oakden, G. J. Stanisz, R. Scott Prosser, F. C. van Veggel, "Size-tunable, ultrasmall $NaGdF_4$ nanoparticles: Insights into their T_1 MRI contrast enhancement," *Chem. Mater.* **23**, 3714–3722 (2011).
81. Y. Hou, R. Qiao, F. Fang, X. Wang, C. Dong, K. Liu *et al.*, "$NaGdF_4$ nanoparticle-based molecular probes for magnetic resonance imaging of intraperitoneal tumor xenografts *in vivo*," *ACS Nano* **7**, 330–338 (2012).
82. K. A. Abel, J.-C. Boyer, Veggel FCv, "Hard proof of the $NaYF_4$/$NaGdF_4$ nanocrystal core/shell structure," *J. Am. Chem. Soc.* **131**, 14644–14645 (2009).
83. Y. Deng, H. Wang, W. Gu, S. Li, N. Xiao, C. Shao *et al.*, "Ho^{3+} doped $NaGdF_4$ nanoparticles as MRI/optical probes for brain glioma imaging," *J. Mater. Chem. B* **2**, 1521–1529 (2014).
84. H. Guo, Z. Li, H. Qian, Y. Hu, I. N. Muhammad, "Seed-mediated synthesis of $NaYF_4$:Yb, Er/$NaGdF_4$ nanocrystals with improved upconversion fluorescence and MR relaxivity," *Nanotechnology* **21**, 125602 (2010).
85. H.-T. Wong, F. Vetrone, R. Naccache, H. L. W. Chan, J. Hao, J. A. Capobianco, "Water dispersible ultra-small multifunctional $KGdF_4$: Tm^{3+}, Yb^{3+} nanoparticles with near-infrared to near-infrared upconversion," *J. Mater. Chem.* **21**, 16589–16596 (2011).
86. G. K. Das, B. C. Heng, S.-C. Ng, T. White, J. S. C. Loo, L. D'Silva *et al.*, "Gadolinium oxide ultranarrow nanorods as multimodal contrast agents for optical and magnetic resonance imaging," *Langmuir* **26**, 8959–8965 (2010).
87. L. Zhou, Z. Gu, X. Liu, W. Yin, G. Tian, L. Yan *et al.*, "Size-tunable synthesis of lanthanide-doped Gd_2O_3 nanoparticles and their applications for optical and magnetic resonance imaging," *J. Mater. Chem.* **22**, 966–974 (2012).
88. X. Kang, D. Yang, Y. Dai, M. Shang, Z. Cheng, X. Zhang *et al.*, "Poly (acrylic acid) modified lanthanide-doped $GdVO_4$ hollow spheres for up-conversion cell imaging, MRI and pH-dependent drug release," *Nanoscale* **5**, 253–261 (2013).
89. M. L. Debasu, D. Ananias, S. L. Pinho, C. F. Geraldes, L. D. Carlos, J. Rocha, "(Gd, Yb, Tb) PO_4 up-conversion nanocrystals for bimodal luminescence-MR imaging," *Nanoscale* **4**, 5154–5162 (2012).
90. S. Zeng, J. Xiao, Q. Yang, J. Hao, "Bi-functional $NaLuF_4$:Gd^{3+}/Yb^{3+}/Tm^{3+} nanocrystals: Structure controlled synthesis, near-infrared upconversion emission and tunable magnetic properties," *J. Mater. Chem.* **22**, 9870–9874 (2012).
91. D. Chen, Y. Yu, F. Huang, H. Lin, P. Huang, A. Yang *et al.*, "Lanthanide dopant-induced formation of uniform sub-10 nm active-core/active-shell nanocrystals with near-infrared to near-infrared dual-modal luminescence," *J. Mater. Chem.* **22**, 2632–2640 (2012).
92. R. Kumar, M. Nyk, T. Y. Ohulchanskyy, C. A. Flask, P. N. Prasad, "Combined optical and MR bioimaging using rare earth ion doped $NaYF_4$ nanocrystals," *Adv. Funct. Mater.* **19**, 853–859 (2009).
93. C.-C. Huang, W. Huang, C.-H. Su, C.-N. Feng, W.-S. Kuo, C.-S. Yeh, "A general approach to silicate nanoshells: Gadolinium silicate and gadolinium silicate: Europium nanoshells for dual-modality optical and MR imaging," *Chem. Commun.* **23**, 3360–3362 (2009).
94. G. Ren, S. Zeng, J. Hao, "Tunable multicolor upconversion emissions and paramagnetic property of monodispersed bifunctional lanthanide-doped $NaGdF_4$ nanorods," *J. Phys. Chem. C* **115**, 20141–20147 (2011).
95. Q. Liu, Y. Sun, C. Li, J. Zhou, C. Li, T. Yang *et al.*, "^{18}F-labeled magnetic-upconversion nanophosphors via rare-earth cation-assisted ligand assembly," *Acs Nano* **5**, 3146–3157 (2011).
96. A. Xia, M. Chen, Y. Gao, D. Wu, W. Feng, F. Li, "Gd^{3+} complex-modified $NaLuF_4$-based upconversion nanophosphors for trimodality imaging of NIR-to-NIR upconversion luminescence, X-Ray computed tomography and magnetic resonance," *Biomaterials* **33**, 5394–5405 (2012).
97. J. Shen, L.-D. Sun, Y.-W. Zhang, C.-H. Yan, "Superparamagnetic and upconversion emitting Fe_3O_4/$NaYF_4$:Yb, Er hetero-nanoparticles via a crosslinker anchoring strategy," *Chem. Commun.* **46**, 5731–5733 (2010).
98. F. Chen, S. Zhang, W. Bu, X. Liu, Y. Chen, Q. He *et al.*, "A neckformation strategy for an antiquenching magnetic/upconversion fluorescent bimodal cancer probe," *Chemistry* **16**, 11254–112560 (2010).
99. Y. Sun, M. Yu, S. Liang, Y. Zhang, C. Li, T. Mou *et al.*, "Fluorine-18 labeled rare-earth nanoparticles for positron emission tomography (PET) imaging of sentinel lymph node," *Biomaterials* **32**, 2999–3007 (2011).
100. Y. Sun, X. Zhu, J. Peng, F. Li, "Core–shell lanthanide upconversion nanophosphors as four-modal probes for tumor angiogenesis imaging," *ACS Nano* **7**, 11290–11300 (2013).

101. J. Peng, Y. Sun, Q. Liu, Y. Yang, J. Zhou, W. Feng *et al.*, "Upconversion nanoparticles dramatically promote plant growth without toxicity," *Nano Res.* **5**, 770–782 (2012).
102. T. Cao, Y. Yang, Y. Sun, Y. Wu, Y. Gao, W. Feng *et al.*, "Biodistribution of sub-10 nm PEG-modified radioactive/upconversion nanoparticles," *Biomaterials* **34**, 7127–7134 (2013).
103. J. Peng, Y. Sun, L. Zhao, Y. Wu, W. Feng, Y. Gao *et al.*, "Polyphosphoric acid capping radioactive/upconverting $NaLuF_4$:Yb, Tm, ^{153}Sm nanoparticles for blood pool imaging *in vivo*," *Biomaterials* **34**, 9535–9544 (2013).
104. Y. Sun, Q. Liu, J. Peng, W. Feng, Y. Zhang, P. Yang *et al.*, "Radioisotope post-labeling upconversion nanophosphors for *in vivo* quantitative tracking," *Biomaterials* **34**, 2289–2295 (2013).
105. M. He, P. Huang, C. Zhang, H. Hu, C. Bao, G. Gao *et al.*, "Dual phase-controlled synthesis of uniform lanthanide-doped $NaGdF_4$ upconversion nanocrystals via an OA/ionic liquid two-phase system for *in vivo* dual-modality imaging," *Adv. Funct. Mater.* **21**, 4470–4477 (2011).
106. Y. Liu, K. Ai, J. Liu, Q. Yuan, Y. He, L. Lu, "A high-performance ytterbium-based nanoparticulate contrast agent for *in vivo* X-ray computed tomography imaging," *Angew. Chem. Int. Ed. Engl.* **51**, 1437–1442 (2012).
107. H. Xing, W. Bu, Q. Ren, X. Zheng, M. Li, S. Zhang *et al.*, "A $NaYbF_4$: Tm^{3+} nanoprobe for CT and NIR-to-NIR fluorescent bimodal imaging," *Biomaterials* **33**, 5384–5393 (2012).
108. L. Cheng, K. Yang, Y. Li, J. Chen, C. Wang, M. Shao *et al.*, "Facile preparation of multifunctional upconversion nanoprobes for multimodal imaging and dual-targeted photothermal therapy," *Angew. Chem. Int. Ed. Engl.* **123**, 7523–7528 (2011).
109. H. Xing, W. Bu, S. Zhang, X. Zheng, M. Li, F. Chen *et al.*, "Multifunctional nanoprobes for upconversion fluorescence, MR and CT trimodal imaging," *Biomaterials* **33**, 1079–1089 (2012).
110. Q. Xiao, W. Bu, Q. Ren, S. Zhang, H. Xing, F. Chen *et al.*, "Radiopaque fluorescence-transparent TaO_x decorated upconversion nanophosphors for *in vivo* CT/MR/UCL trimodal imaging," *Biomaterials* **33**, 7530–7539 (2012).
111. G. Zhang, Y. Liu, Q. Yuan, C. Zong, J. Liu, L. Lu, "Dual modal *in vivo* imaging using upconversion luminescence and enhanced computed tomography properties," *Nanoscale* **3**, 4365–4371 (2011).
112. J.-W. Shen, C.-X. Yang, L.-X. Dong, H.-R. Sun, K. Gao, X.-P. Yan, "Incorporation of computed tomography and magnetic resonance imaging function into $NaYF_4$:Yb/Tm upconversion nanoparticles for *in vivo* trimodal bioimaging," *Analy. Chem.* **85**, 12166–12172 (2013).
113. Z. Gu, L. Yan, G. Tian, S. Li, Z. Chai, Y. Zhao, "Recent advances in design and fabrication of upconversion nanoparticles and their safe theranostic applications," *Adv. Mater.* **25**, 3758–3779 (2013).
114. G. Tian, X. Zhang, Z. Gu, Y. Zhao, "Recent advances in upconversion nanoparticles-based multifunctional nanocomposites for combined cancer therapy," *Adv. Mater.* **27**, 7692–7712 (2015).
115. A. Zhou, Y. Wei, Q. Chen, D. Xing, "*In vivo* near-infrared photodynamic therapy based on targeted upconversion nanoparticles," *J. Biomed. Nanotechnol.* **11**, 2003–2010 (2015).
116. H. S. Qian, H. C. Guo, P. C. L. Ho, R. Mahendran, Y. Zhang, "Mesoporous-Silica-coated up-conversion fluorescent nanoparticles for photodynamic therapy," *Small* **5**, 2285–2290 (2009).
117. B. Ungun, R. K. Prud'Homme, S. J. Budijon, J. Shan, S. F. Lim, Y. Ju *et al.*, "Nanofabricated upconversion nanoparticles for photodynamic therapy," *Opt. Express* **17**, 80–86 (2009).
118. P. Zhang, W. Steelant, M. Kumar, M. Scholfield, "Versatile photosensitizers for photodynamic therapy at infrared excitation," *J. Am. Chem. Soc.* **129**, 4526–4527 (2007).
119. Y. Guo, M. Kumar, P. Zhang, "Nanoparticle-based photosensitizers under CW infrared excitation," *Chem. Mater.* **19**, 6071–6072 (2007).
120. J. Shan, S. J. Budijono, G. Hu, N. Yao, Y. Kang, Y. Ju *et al.*, "Pegylated composite nanoparticles containing upconverting phosphors and meso-tetraphenyl porphine (TPP) for photodynamic therapy," *Adv. Funct. Mater.* **21**, 2488–2495 (2011).
121. G. Tian, W. Ren, L. Yan, S. Jian, Z. Gu, L. Zhou *et al.*, "Red-emitting upconverting nanoparticles for photodynamic therapy in cancer cells under near-infrared excitation," *Small* **9**, 1929–1938 (2013).
122. S. Cui, D. Yin, Y. Chen, Y. Di, H. Chen, Y. Ma *et al.*, "*In vivo* targeted deep-tissue photodynamic therapy based on near-infrared light triggered upconversion nanoconstruct," *ACS Nano* **7**, 676–688 (2012).
123. F. Wang, D. Banerjee, Y. Liu, X. Chen, X. Liu, "Upconversion nanoparticles in biological labeling, imaging, and therapy," *Analyst* **135**, 1839–1854 (2010).
124. M. E. Gindy, R. K. Prud'homme, "Multifunctional nanoparticles for imaging, delivery and targeting in cancer therapy," *Expert Opin Drug* **6**, 865–878 (2009).
125. C. Wang, L. Cheng, Z. Liu, "Drug delivery with upconversion nanoparticles for multi-functional

targeted cancer cell imaging and therapy," *Biomaterials* **32**, 1110–1120 (2011).
126. N. M. Idris, M. K. Gnanasammandhan, J. Zhang, P. C. Ho, R. Mahendran, Y. Zhang, "*In vivo* photodynamic therapy using upconversion nanoparticles as remote-controlled nanotransducers," *Nat. Med.* **18**, 1580–1585 (2012).
127. C. Wang, H. Tao, L. Cheng, Z. Liu, "Near-infrared light induced *in vivo* photodynamic therapy of cancer based on upconversion nanoparticles," *Biomaterials* **32**, 6145–6154 (2011).
128. Z. Zhao, Y. Han, C. Lin, D. Hu, F. Wang, X. Chen *et al.*, "Multifunctional core-shell upconverting nanoparticles for imaging and photodynamic therapy of liver cancer cells," *Chemistry.* **7**, 830–837 (2012).
129. B. Dong, S. Xu, J. Sun, S. Bi, D. Li, X. Bai *et al.*, "Multifunctional $NaYF_4$:Yb^{3+}, Er^{3+}@Ag core/shell nanocomposites: Integration of upconversion imaging and photothermal therapy," *J. Mater. Chem.* **21**, 6193–6200 (2011).
130. Q. Xiao, X. Zheng, W. Bu, W. Ge, S. Zhang, F. Chen *et al.*, "A core/satellite multifunctional nanotheranostic for *in vivo* imaging and tumor eradication by radiation/photothermal synergistic therapy," *J. Am. Chem. Soc.* **135**, 13041–13048 (2013).
131. H. Xu, L. Cheng, C. Wang, X. Ma, Y. Li, Z. Liu, "Polymer encapsulated upconversion nanoparticle/iron oxide nanocomposites for multimodal imaging and magnetic targeted drug delivery," *Biomaterials* **32**, 9364–9373 (2011).
132. Z. Hou, C. Li, P. Ma, G. Li, Z. Cheng, C. Peng *et al.*, "Electrospinning preparation and drug-delivery properties of an up-conversion luminescent porous $NaYF_4$:Yb^{3+}, Er^{3+}@Silica fiber nanocomposite," *Adv. Funct. Mater.* **21**, 2356–2365 (2011).
133. Z. Xu, C. Li, Z. Hou, D. Yang, X. Kang, J. Lin, "Facile synthesis of an up-conversion luminescent and mesoporous Gd_2O_3:Er^{3+}@$nSiO_2$@$mSiO_2$ nanocomposite as a drug carrier," *Nanoscale* **3**, 661–667 (2011).
134. J. V. Garcia, J. Yang, D. Shen, C. Yao, X. Li, R. Wang *et al.*, "NIR-triggered release of caged nitric oxide using upconverting nanostructured materials," *Small* 8, 3800–3805 (2012).
135. P. T. Burks, J. V. Garcia, R. GonzalezIrias, J. T. Tillman, M. Niu, A. A. Mikhailovsky *et al.*, "Nitric oxide releasing materials triggered by near-infrared excitation through tissue filters," *J. Am. Chem. Soc.* **135**, 18145–18152 (2013).
136. X. Zhang, G. Tian, W. Yin, L. Wang, X. Zheng, L. Yan *et al.*, "Controllable generation of nitric oxide by near-infrared-sensitized upconversion nanoparticles for tumor therapy," *Adv. Funct. Mater.* **25**, 3049–3056 (2015).
137. S. Jiang, Y. Zhang, "Upconversion nanoparticle-based FRET system for study of siRNA in live cells," *Langmuir* **26**, 6689–6694 (2010).
138. M. K. G. Jayakumar, N. M. Idris, Y. Zhang, "Remote activation of biomolecules in deep tissues usingnear-infrared-to-UV upconversion nanotransducers," *Proc. Nat. Acad. Sci. U.S.A.* **109**, 8483–8488 (2012).
139. T. Zhou, X. Zhou, D. Xing, "Controlled release of doxorubicin from graphene oxide based charge-reversal nanocarrier," *Biomaterials* **35**, 4185–4194 (2014).
140. R. A. Jalil, Y. Zhang, "Biocompatibility of silica coated $NaYF_4$ upconversion fluorescent nanocrystals," *Biomaterials* **29**, 4122–4128 (2008).
141. J. Zhou, Y. Sun, X. Du, L. Xiong, H. Hu, F. Li, "Dual-modality *in vivo* imaging using rare-earth nanocrystals with near-infrared to near-infrared (NIR-to-NIR) upconversion luminescence and magnetic resonance properties," *Biomaterials* **31**, 3287–3295 (2010).